Conference Proceedings

EuroSun 2016
Palma de Mallorca (Spain), 11 - 14 October 2016

Competitive Assessment between Solar Thermal and Photovoltaics for Industrial Process Heat Generation

Steven Meyers, Bastian Schmitt, and Klaus Vajen

[1] Institute of Thermal Engineering, University of Kassel, Kassel, Germany

Abstract

The interest in photovoltaic heating has grown in recent years due to falling technology costs and ease of installation, though mainly in the residential sector. A study was conducted to determine under which conditions photovoltaic heating may become less expensive than solar thermal in low temperature industry (e.g. food and beverage). A broad parametric simulation study was conducted in TRNSYS which determined specific energetic yields for solar thermal and photovoltaic heating systems. A comparative analysis followed suit, conducted in a way to generate an assessment tool which functions for nearly every industrial, climatic, or economic setting. Results indicated that for lower temperature applications, solar thermal will remain a preferred choice in most climates. For higher temperature industrial process heat requirements, photovoltaic heating may already provide a lower cost solution in low and medium solar irradiation climates.

Keywords: *renewable heat, solar thermal, photovoltaic, process heat*

1. Introduction

In the wake of COP 21, nations across the world agreed to begin reducing their carbon emissions, namely through renewable electricity and lower carbon transport. While important, it overlooks an equally relevant carbon emitting sector, industrial manufacturing, which consumes mainly thermal energy. Lower carbon heat can be achieved through a few mechanisms, but solar offers the nearest term and most complete solution for the quickest reduction. Solar thermal (ST) collectors are an obvious choice for obtaining thermal energy, but in some niche markets photovoltaic (PV) heating systems are now being offered. While their focus is primarily on the domestic hot water sector, it provides an example where PV electrical resistance heating may be more cost effective than solar thermal.

The choice for PV resistance heating is easy to understand. The costs continue to drop year after year, installation is nearly fail proof, and its thermal energy generation capability is nearly independent of the process temperature level. Until now, minimal research (Fanney and Dougherty, 1997; Le Berre et al., 2014) has been done to compare the thermal energy generation costs of ST and PV at various temperature levels. Therefore, an assessment was conducted to determine their specific energy generation capabilities, paying close attention to their cost competitiveness for various climates, industrial process temperatures, load profiles and storage tank sizes.

2. Methodology

Two simulation decks were constructed in TRNSYS 17 to obtain the energetic yield potential of solar thermal and solar photovoltaic heating systems under various boundary conditions. Specific energy yields (per m^2 for ST and per W_p for PV) were then used to calculate the Levelized Cost of Heat (LCOH),

doi:10.18086/eurosun.2016.02.01 Available at http://proceedings.ises.org

subsequently used to determine the Cost Ratio (CR), an inflection point which indicated a preferred heating technology.

2.1. Solar Thermal Heating Model

The TRNSYS thermodynamic model was constructed around the popularly used collector model Type 832 (v5.01), developed by Haller et al. (2013), shown in Fig. 1. A constant speed pump in the solar loop operated between an upper and lower deadband of 7 K and 3 K between the collector (T_{coll}) and the bottom storage tank temperature ($T_{0.1}$), respectively. Connected pipes, insulation, charging/discharging heat exchangers and pump flow rates in the loops were sized in accordance to VDI 6002 (VDI, 2014). A storage tank was included (Type 534) to allow for flexibility in heat storage and delivery. For the charging loop, the storage tank had two inlet valves, located at a relative height of 0.9 and 0.6 from the bottom, allowing for stratification, as well as an outlet at 0.1. A constant speed pump in the charging loop was activated using the same deadband as the solar loop, though comparing temperatures between the heat exchanger ($T_{solarHX}$) and the bottom storage tank temperature ($T_{0.1}$). The process discharge loop was activated when the temperature difference between storage tank ($T_{0.9}$) and process return ($T_{process\ return}$) was greater than 10 K and deactivated at 5K. Temperature controls were put into place for the collector and storage tank, protecting both from stagnation and overheating. The discharge flowrate ($\dot{m}_{discharge}$) was regulated by a Type 805 heat exchanger (Heimrath and Haller, 2007), controlling the process flow temperature ($T_{process\ flow}$) to its set temperature when possible. If not achievable due to insufficient stored energy, the pump was operated at its maximum flow rate, which was set at 90% of the maximum flow rate of the process. The process was defined in section 2.3.

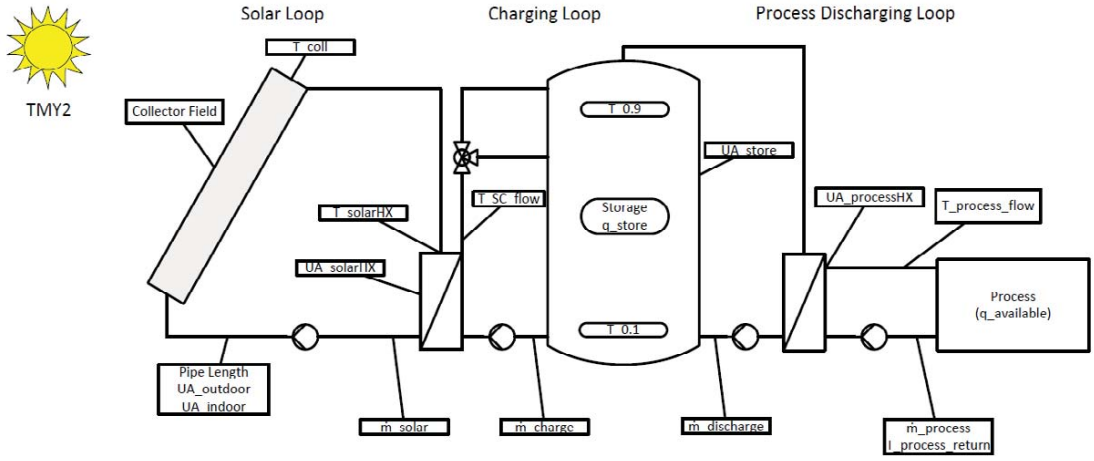

Fig. 1: The design of the solar thermal heating model in TRNSYS

2.2. Photovoltaic Heating Model

The solar loop for the PV heating model was built using Type 562, with inputs modelled after a high efficiency mono-silicon module, shown in Fig. 2. Two resistance heaters were implemented to directly heat the process fluid or water in the storage tank with an assumed efficiency of 98%. If the process load heating requirement ($q_{available}$) was greater than the available energy produced by the PV solar loop (q_{pv}), all electrical energy was directed to the process resistance heater. If excess energy was available, it was sent to the charging loop (storage) resistance heater. The charging loop variable speed pump adjusted the flow rate ($\dot{m}_{charge}$) to store the heat (Type 534) with high stratification. The discharge mass flow rate ($\dot{m}_{discharge}$) of the storage tank was controlled by determining the difference between $q_{available}$ and q_{pv}. If there was a deficit, the mass flow rate was calculated to heat the difference. This only occurred when there was a 10 K or greater difference between the upper storage tank temperature ($T_{0.9}$) and the process return temperature ($T_{process\ return}$). If the storage tank ever became full while the process load was completely heated by the PV system, any excess energy produced was considered wasted or sent to the local grid.

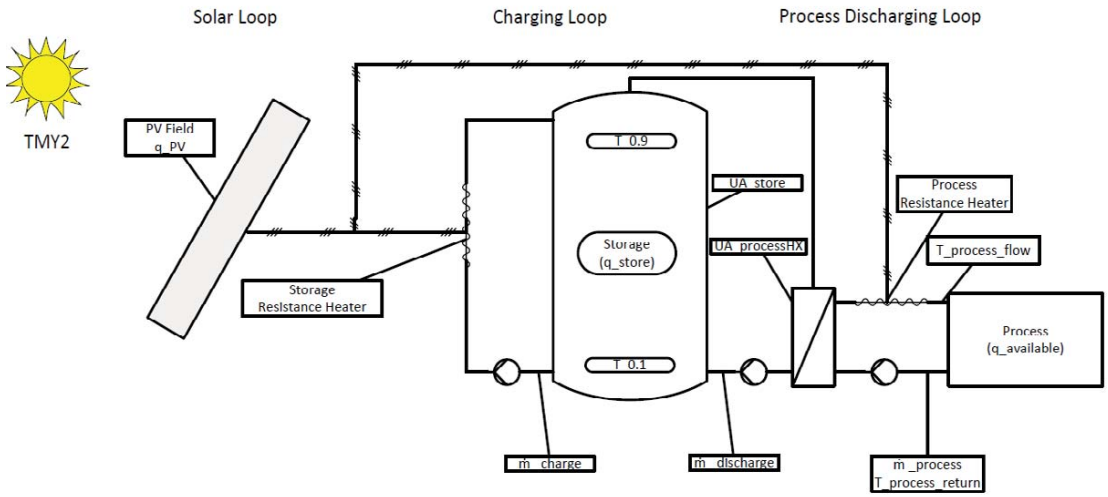

Fig. 2: The design of the solar PV heating model in TRNSYS

2.3. Simulation Parameters and Cases

A large parametric study was conducted to include geographical and industrial manufacturing conditions found all over the world. Quantities have been normalized to allow for easily scalability for specific conditions. For each parametric case, both a ST and PV simulation was conducted and subsequently compared.

Process Load and Profile

The process load quantity and temporal (daily, weekly) profile are two key parameters which have a significant influence on the overall performance of the industrial solar heating system. The load was defined as the daily energetic demand of the process divided by the gross area (A_g) of installed solar collector area (eq. 1). For instance, if the process has a daily flow of 30 m^3 from 45..75 °C with 125 m^2 of installed collectors, the specific daily load was calculated at 8.2 kWh/m^2d. Three various load quantities were simulated for this study, at 4, 6, and 10 kWh/m^2d, which represent a low, medium and high load demand. A load of 20 kWh/m^2d was also simulated to determine an ideal case which all thermal energy was immediately transferred to the load, thus eliminating the need for a storage tank.

$$q_{available} = \dot{V}_{process} \cdot \rho \cdot c_p \cdot \Delta T / A_g = 8.2 \ \frac{kWh}{m^2 d} \qquad \text{(eq. 1)}$$

Multiple daily and weekly load profiles have been recommended by Lauterbach (2014) for various cases found in industry. The best case scenario (highest efficiency) for a solar plant was a constant daily load profile which operates seven days a week (minimal heat losses). The mentioned load profile was partitioned into hourly sections, shown in Fig. 3. The hourly energy load, used in the TRNSYS simulations, was then determined by multiplying the hourly share of daily demand (Fig. 3) by specific daily load ($q_{available}$).

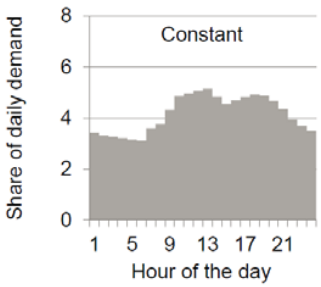

Fig. 3: Simulated daily load profile (Lauterbach, 2014)

Storage Tank Size

The available specific storage tank capacity (q_{store}) was defined by the stored thermal energy between the maximum rated storage tank temperature and the process load return temperature divided by the gross area of the ST system. Lauterbach (2014) recommended a specific storage tank capacity between 3 and 9 kWh/m^2 for low temperature solar thermal systems in central European climates. Due to higher process temperatures

and simulations conducted in higher solar resource regions, the specific storage tank sizes were 3, 5, 7, 9, and 11 kWh/m^2. The storage tank specific volume (v_{store}) was subsequently calculated (eq. 2), which determined the storage tank size capacity, in l/m^2. A typical non-pressurized storage tank had a $T_{0.9max}$ of 95 °C. If the $T_{process\ return}$ was 25 °C and a large q_{store} was desired (9 kWh/m^2), the calculated storage tank specific volume was 112.6 l/m^2.

$$v_{store} = q_{store}/c_p \cdot \rho \cdot \left(T_{0.9max} - T_{process_{return}}\right) = 112.6\ \frac{l}{m^2} \quad \text{(eq. 2)}$$

At higher temperatures, less energy was stored due to the storage tank thermal limitations. As a reference, the maximum storage tank temperatures were as followed (Tab. 1), based upon the process flow temperature.

Tab. 1: The relationship between process flow temperature and maximal allowed storage tank temperature

$T_{process\ flow}$ (°C)	$T_{0.9max}$ (°C)
< 90	95
< 120 and >90	130
>120	$T_{process\ flow}$ + 30

Collectors and Process Temperatures

Four solar thermal collectors (Flat Plate [FPC], Evacuated Tube [ETC], Compound Parabolic Concentrator [CPC], Parabolic Trough [PTC]) and one photovoltaic collector were selected for simulation. Each thermal collector was simulated at three temperature ranges, fitting for their potential applications in industry while the single PV collector covered all noted temperature ranges, as is the nature of electric heating. The ST collector model (Type 832V5.01) implemented the quasi-dynamic testing method (EN 12975-2 and ISO 9806:2013) for the parameters used by TRNSYS (Tab. 2). The PV model parameters (Type 562) were provided by the manufacturer (Tab. 3). All parameters are in terms of gross area, A_g. Incident Angle Modifiers (IAM, transverse, longitudinal, and diffuse) were also implemented.

Tab. 2: Solar thermal collector simulation parameters and load temperatures

		FPC	ETC	CPC	PTC
η_o (-)		0.77	0.48	0.56	0.59
c_1 (W/m^{2}K)		3.25	1.21	0.78	0.21
c_2 (W/m^{2}K^2)		0.0150	0.0038	0.0009	0.0013
c_5 (J/m^{2}K)		4425	12870	7379	1906
Process 1 (°C)	Return	30	45	60	75
	Flow	60	75	90	105
Process 2 (°C)	Return	45	60	75	90
	Flow	75	90	105	120
Process 3 (°C)	Return	60	75	90	110
	Flow	90	105	120	140

Tab. 3: Solar PV collector simulation parameters, G_T is defined as the incident irradiation on the tilted collector surface

	PV (Mono-silicon)
Reference Efficiency (%) at 25 °C and G_T:1000 W/m^2	19
Temperature Efficiency Modifier (1/C)	-0.0038
Radiation Efficiency Modifier (%)	$0.0502 \cdot \ln(G_T)+0.6833$

Locations

It was critical to select simulation sites whose results can provide analysis for nearly every location in the world. The two main factors which affected the performance of ST and PV systems were the daytime ambient temperature ($T_{amb,day}$) and diffuse ratio ($DR=H_d/H_t$). Given three levels (low, medium, and high) of both, nine sites were selected from the extended weather database in TRNSYS to conduct the parametric study, shown in Tab. 4. Fig. 4 included these nine sites, plotted in a line by similar diffuse ratios (indicated in Tab. 4), along with 1079 other sites within the TRNSYS database, which indicated how these nine sites provided representation for nearly all global climate conditions.

Tab. 4: The selected sites for simulation analysis, detailing their solar irradiation, average daytime ambient temperature, diffuse ratio, and latitude

Site	GHI (kWh/m²a)	DNI (kWh/m²a)	$T_{amb,day}$ (°C)	DR	Latitude (°)
Dongola, Sudan	2476	2843	29.8	0.22 (low)	19.17
Jerusalem	2093	2404	18.3	0.26 (low)	31.78
Eagle, Colorado, USA	1715	2031	9.6	0.33 (low)	39.65
Abu Dhabi, UAE	1957	1605	29.2	0.45 (mid)	24.43
Sydney, Australia	1608	1450	19.5	0.46 (mid)	-33.87
Kursk, Russia	1222	1334	9.1	0.46 (mid)	51.77
Copenhagen, Denmark	988	899	10.6	0.56 (high)	55.67
Bologna, Italy	1201	894	16.8	0.57 (high)	44.53
Kuching, Malaysia	1603	907	27.4	0.60 (high)	1.15

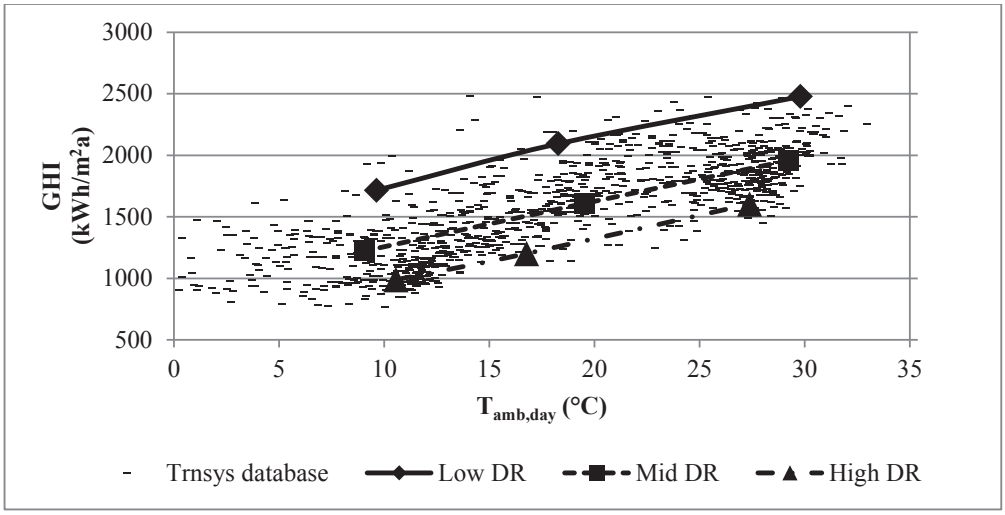

Fig. 4: Illustration of the nine selected sites for simulation, plotted in three lines respective of their DR levels, along with other sites found in the TRNSYS database

Simulation Setup and Key Results

The ST model was validated by comparing results to a similar model created by Lauterbach (2014) (validated on a solar process heat plant at a brewery in Germany), which yielded a system utilization ratio difference of less than -2%. The PV model used the same main components (pipes, storage tank, insulation, heat exchangers), only replacing the solar heating source. While not directly validated, it serves as a good approximation as what may be installed in the future, as no PV process heat plant is currently in operation.

The ST and PV parametric simulations were conducted using TRNEdit, once the TRNSYS simulation deck was finalized. Completed annual simulations recorded key variables such as the specific annual system yield (eq. 3), the annual system utilization ratio (eq. 4), and the solar fraction (eq. 5). The specific annual system yield was defined by the total energy delivered to the process load from the ST or PV system, taking into

account thermal losses of the hydraulics and storage tank. The annual utilization ratio was determined by dividing the specific annual system yield by the quantity of useable solar irradiation on the collector surface during the year (total or beam). The solar fraction was calculated by the dividing the specific annual system yield by the annual specific load.

$$Q_{yield}^{ST,PV} = \sum_0^{8760} \Delta Q_{process} \quad \text{(eq. 3)}$$

$$\eta_{system}^{ST,PV} = Q_{yield}^{ST,PV} / H_{t,b} \quad \text{(eq. 4)}$$

$$f_{sol}^{ST,PV} = Q_{yield}^{ST,PV} / \sum_0^{8760} q_{available} \quad \text{(eq. 5)}$$

There was an inherent mismatch between the standard units of ST and PV systems, as ST specific performance and costs are commonly per square meter and PV per watt peak (W_p). While these respective units are used in subsequent comparative analysis, a conversion was made between the two to ensure that both thermal systems have the same parameters (i.e. $q_{available}$, q_{store}) while being simulated. The peak specific energy yield by the ST system was estimated using the simulated collector parameters and expected mean collector temperature (Tab. 2). A similarly sized (by energy) PV system was then determined by dividing the ST peak specific energy yield by the nominal PV efficiency. For example, if a ST system generated 0.6 kW/m^2 for a given process temperature while assuming a 19% nominal efficiency of the PV system (0.19 kW/m^2), the simulated PV system must have gross surface area 3.15 times lager to yield the same peak thermal energy (input into TRNSYS). Through this, the previously mentioned specific simulation parameters can be used by both the ST and PV models, allowing for an equal comparison.

2.4. Energetic and Cost Comparisons

The Levelized Cost of Heat (LCOH) is a standard metric used when comparing two or more technology types to determine which has the lowest heat generation cost over a certain time period. Absolute LCOH values are important to determine when building solar systems, but for a comparison study relative costs are more insightful and allow for flexibility for multiple cost conditions.

The LCOH for both the ST and PV systems is shown in (eq. 6) with key parameters listed in Tab. 5.

$$LCOH = \frac{CapEx_{ST,PV} + \sum_{n=1}^{20} \frac{OM_{ST,PV}}{(1+DR)^n}}{\sum_{n=1}^{20} \frac{Q_{yield}^{ST,PV} * (1-SD)^n}{(1+DR)^n}} \quad \text{(eq. 6)}$$

Tab. 5: The input parameters to calculate the Levelized Cost of Heat

Parameter	Definition	ST Value	PV Value
$CapEx_{ST,PV}$	Capital Expenditure (€/m^2 or €/W_p)	Variable	Variable
$OM_{ST,PV}$	Operation and Maintenance (€/m^2 or €/W_p)	2% of CapEx	1% of CapEx
DR	Discount Rate	3.50%	3.50%
SD	Degradation Rate	1.0%	0.5%
n	Years of Operation	20	20

The LCOH Ratio was defined by the division of the LCOH of the ST system by that of the PV system for the same simulation case (eq. 7). This value was required to help calculate the Cost Ratio and also serves as an indicator to the lower cost solar heat system. When this value is greater than one, the heat generated from the PV system is less expensive, and when less than one, the heat from the ST system is.

$$LCOH_{ratio}(LHR) = \frac{LCOH_{ST}}{LCOH_{PV}} \quad \text{(eq. 7)}$$

If the $LCOH_{ratio}$ is set to one, it can be rearranged ($LCOH_{ST} = LCOE_{PV}$) and reformulated to determine the Cost Ratio (CR) (eq. 8), which is the $CapEx_{ST}$ divided by $CapEx_{PV}$. To do this, an assumed $CapEx_{PV}$ was input into the equation, along with the known annual ST and PV system yields. An iterative loop was written

in Matlab to determine the $CapEx_{ST}$ which makes $LCOH_{ST}$ = $LCOE_{PV}$ true, providing both inputs to determine the Cost Ratio, which was calculated for every parametric run.

$$CR = \frac{CapEx_{ST}}{CapEx_{PV}} \left(\frac{W_p}{m^2}\right), when\ LHR = 1 \quad \text{(eq. 8)}$$

For example, in a particular simulation the specific ST yield was 452 kWh/m^2 and the PV 1001 kWh/kWp. Using (eq. 6) with parameters from Tab. 5 and an assumed $CapEx_{PV}$ of 1.5 €/W_p (Shah and Booream-Phelps, 2015), the iterated $CapEx_{ST}$ was 576 €/m^2, leading to a CR of 384 W_p/m^2. When doing the same iteration under various $CapEx_{PV}$, the same CR was calculated.

The advantage of the CR is that it allows the comparative analysis in any currency to be flexible for the ever changing $CapEx_{ST,PV}$, whether it is from technology/system improvements or changes in local subsidies. It is used in two ways: either one CapEx is known and the other is determined using the simulated CR; or both $CapEx_{ST,PV}$ are known and are compared against the simulated CR. For the first case, the $CapEx_{PV}$ tends to be less variable than that of ST, due to the commoditization of PV panels and is for example purposes, set at 1.3 €/W_p. Assuming a simulated CR of 384 W_p/m^2, these two values are multiplied together to determine the maximum cost of a comparable ST system (eq. 9) for it to be financially competitive with the PV system. For the second case, if both CapExs are known (450 €/m^2 and 1.6 €/W_p), the CR is calculated to be 281 W_p/m^2 (eq. 10) and when less than simulated CR, ST produced heat at a lower cost.

$$1.3 \frac{€}{W_p} \cdot 384 \frac{W_p}{m^2} = 499 \frac{€}{m^2} \quad \text{(eq. 9)}$$

$$450 \frac{€}{m^2} / 1.6 \frac{€}{W_p} = 281 \frac{W_p}{m^2} \quad \text{(eq. 10)}$$

Graphical representation of the CR as a function of solar irradiation and ambient temperature were constructed per simulation case to serve as an easy to use guide to determine which industrial solar heating system has the lowest cost.

3. Simulation Results

3.1. Energy Yields and Cost Ratios

Three simulation sites are shown to illustrate the type of results obtained from the parametric study with indicated process temperatures and selected ST technology. The first site was Copenhagen (FPC), the second Sydney (CPC), and the final Abu Dhabi (PTC) (Fig.5). For this example, the process load ($q_{available}$) was 6 kWh/m^{2}d and storage tank size (q_{store}) 9 kWh/m^2, indicating a medium load and large store. The process temperatures for each case are noted on the x-axis. The primary y-axis shows the system utilization ratio (η_{system}) and the secondary the associated Cost Ratio (CR).

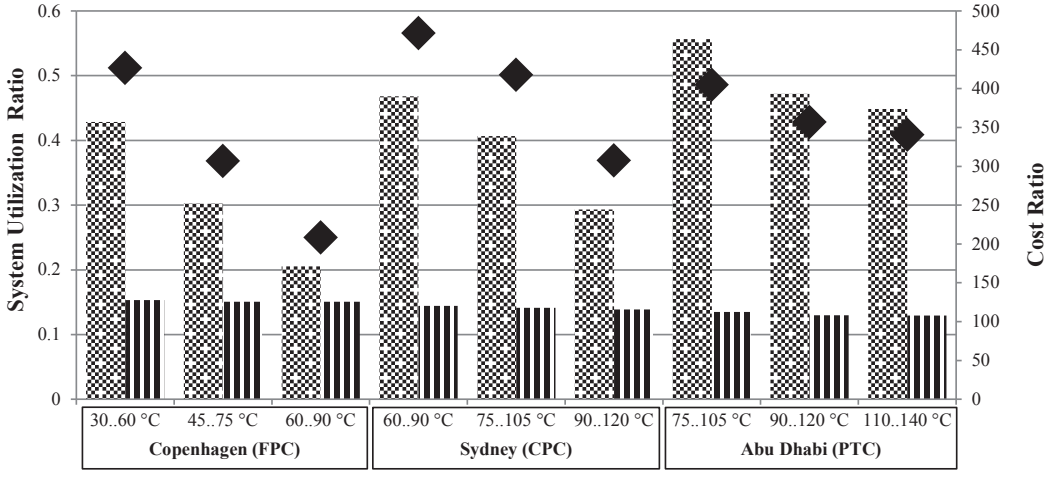

Fig. 5: Three exemplary sites showcasing the ST and PV system utilization ratios and Cost Ratio for three temperature levels and ST technologies

3.2. Comparison Graphs

To graphically compare ST and PV heating systems, new plots were constructed with the CR on the x-axis and the respective available solar irradiation on the y-axis for the nine sites during one parametric simulation (one collector, process temperature, load, and storage tank size). Sites with similar ambient daytime temperatures (Low~10°C, Medium~18°C, High~28°C) were connected with lines, which represent LHR lines. The CR and GHI cases above this line represents situations when the LHR<1, indicating that heat generated by a ST system is less expensive, and the contrary below said line. Fig. 6 shows a lower temperature case with FPC while Fig. 7 was for a higher temperature case with PTC. The previously mentioned sites are circled in each figure as a reference.

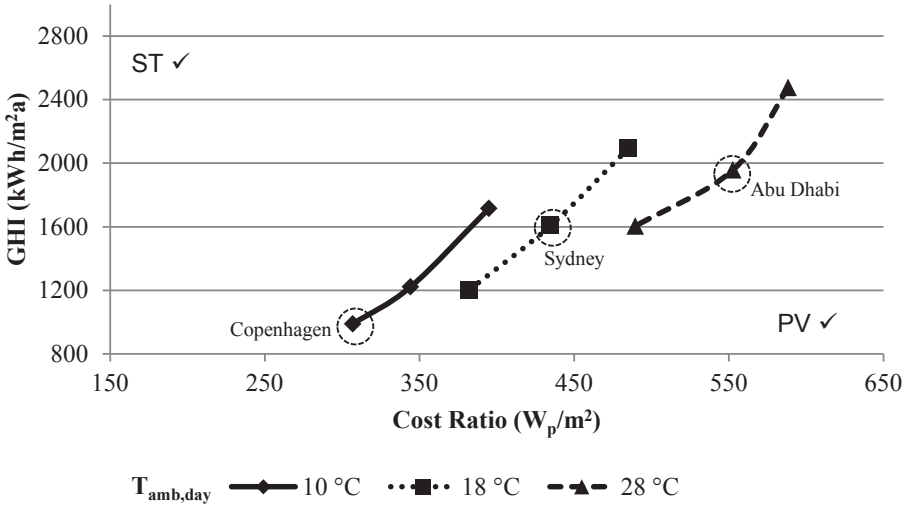

Fig. 6: Solar Thermal and PV comparison graph for a FPC with a process of 45..75 °C, specific load of 6 kWh/m²d, and specific store of 9 kWh/m²

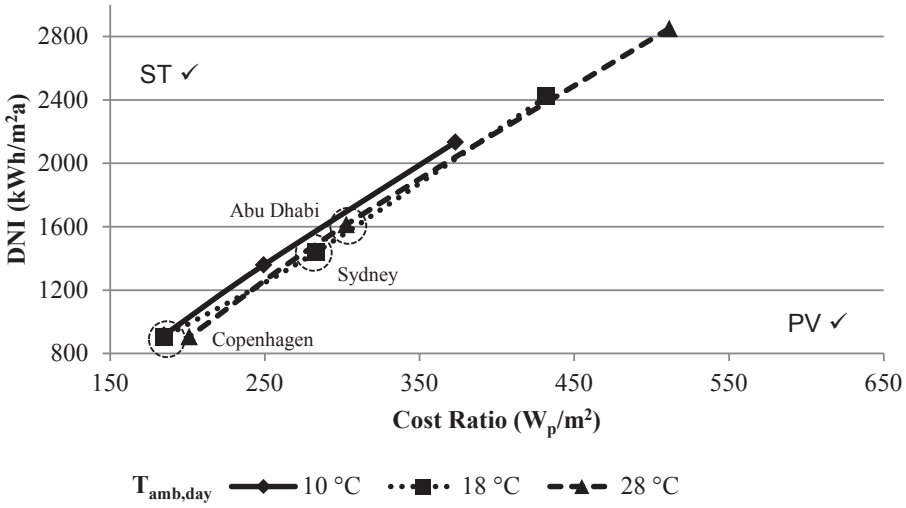

Fig. 7: Solar Thermal and PV comparison graph for a PTC with a process of 110..140 °C, specific load of 10 kWh/m²d, and specific store of 9 kWh/m²

3.3. Example Application of Comparison Graphs

The use of the comparison graphs provided a powerful yet easy to understand tool to determine which industrial solar heating technology can provide a lower cost of heat. As an example case, Fig. 8 detailed two ST collectors (FPC, CPC) for one case (process temperatures 60..90 °C, load 6 kWh/m²d, store 7 kWh/m²);

something which may happen in reality when deciding between different collectors for a system. Tab. 6 highlighted four technology comparisons for two different locations along with the determined CR by using Fig. 8. This was done per site by drawing a horizontal line from the y-axis at the corresponding GHI to the fitting temperature line (or interpreted between two lines) of the desired ST technology. From this point, a vertical line was drawn to the x-axis, which determined the CR for that case. The CR was then used, as in (eq. 9), to determine the competitive maximum cost of a ST system by simply multiplying the known PV cost (€/W_p) by the Cost Ratio (W_p/m^2) (Tab. 6). If a Cost Ratio was already known through local ST and PV costs, the comparison can be done in reverse. A vertical line could be drawn up from the x-axis and a horizontal line right from the y-axis (given the local solar irradiation). The intersection point of these two lines was compared to the local temperature line (the LHR line). If this point was above the line, ST was a better choice (indicated by the ST check mark in the upper left hand corner). If below the curve, PV was selected (PV check mark in the lower right hand corner).

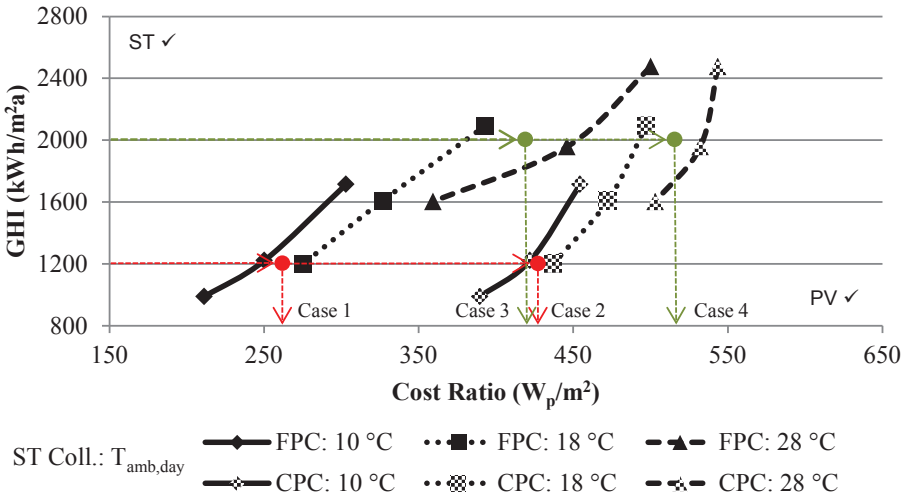

Fig. 8: An example of how to use the comparison graphs to determine the Cost Ratio for specific locations and system cases. These plots are valid for process temperatures 60..90 °C, load 6 kWh/m²d, and store 7 kWh/m²

Tab. 6: Input parameters and results for use in the comparison graph example in Fig. 8

Case	Site	GHI (kWh/m²a)	$T_{amb,day}$ (°C)	ST Technology	CR (W_p/m^2)	PV Cost (€/W_p)	ST Max. Cost (€/m²)
1	1	1200	14	FPC	265	1.2	318
2	1	1200	14	CPC	430	1.2	516
3	2	2000	23	FPC	420	1.5	630
4	2	2000	23	CPC	515	1.5	773

4. Discussion

The resulting energetic simulations in TRNSYS revealed the expected results for the both the ST and PV heating systems. For all three presented cases (Fig. 5), the ST system utilization ratio decreased as a function of process temperature, due to increased collector thermal losses. While three different technologies were used for Copenhagen, Sydney, and Abu Dhabi, it was clearly shown that ambient temperature plays a large role in the effectiveness of such collectors, as Abu Dhabi's showed the highest average system utilization factor and Copenhagen the lowest. The opposite was true for the PV systems, where a lower system utilization ratio occurred in the higher irradiation regions, namely due to greater ambient temperatures and the technology's negative temperature efficiency modifier. The higher process temperature PV systems showed a small decrease in performance due to larger thermal losses in the storage tank. Combining these two trends together, it was understandable that the Cost Ratio for all ST technologies decreased as a function of process temperature. The rate of decrease was less for the PTC and CPC, as both technologies had smaller thermal losses (c_1, c_2) and are more immune to reduced performance at higher process temperatures.

The results shown in Fig.6 and Fig.7 demonstrated the goals of this research, to create an easily understood graph which helps determine the preferred renewable solar heating technology; no matter where it is geographically located, when it may be built, and which currency is used. Analysis of this graph determined clear trends which are supported by other simulations not detailed in this paper. The best conditions for ST systems are exhibited in Fig. 6, for a lower temperature heating process load met using relatively inexpensive FPC. In higher temperature regions with high solar irradiation like Abu Dhabi, given present and future PV costs, it does not seem likely that PV would ever overtake ST. In lower temperature and solar regions like Copenhagen, PV heating may pose a near term threat. This was mainly due the location's numerous cold and cloudy days in which no energy was produced by ST while PV still could, actually benefiting from the colder temperatures and having a lower minimum solar irradiance requirement for energy production. The contrary was shown in Fig. 7, the situation where PV may soon, if not already, overtake ST as the preferred industrial solar heating choice. For higher temperature processes requiring a concentrating collector, all three temperature lines are shifted left towards the y-axis, indicating a decreased Cost Ratio and thus more competitive PV system. This can be a challenge, as concentrating collectors tend to be more expensive than other solar thermal technologies. If PV costs were assumed to be 1 €/W_p, then even in regions with a DNI resource of greater than 2000 kWh/m^2a, the installed cost of a PTC system must be less 400..500 €/m^2, difficult given their current estimated costs (Frank et al., 2013).

5. Conclusion and Future Work

This study was conducted in order to provide insight into the future of industrial process heating by solar energy. Traditionally, this has been done with solar thermal collectors. However, with the continued development of lower cost PV systems and their inherent ease of installation, this technology may prove to provide a lower cost source of low carbon heat. Through energetic simulations and comparative financial analysis, it was shown that for lower temperature process heat cases, solar thermal systems will most likely remain the preferred technology choice. The contrary was true for higher temperature applications, especially in colder, lower solar resource locations, where PV is already a competitive choice for heat generation. The exhibited results were crafted in such a way that they can be used for nearly any industrial process heat condition, global location, and present or future technology cost. The opportunity cost of not using PV energy for offsetting local electricity consumption was not considered. This is one avenue of future work, along with the assessment of industrial heat pumps working together with ST and PV to provide the lowest carbon emission heat source for industrial applications.

6. Acknowledgements

The authors wish to acknowledge the European Union for funds received through the People Programme (Marie Curie Actions) of the Seventh Framework Programme FP7/2007-2013/ under REA grant agreement n° 317085 (PITN-GA-2012-317085), commonly known at the SHINE (Solar Heat INtegration Network) Program (https://www.uni-kassel.de/projekte/solnet-shine/home.html).

7. References

Fanney, A. H. and Dougherty, B. P., 1997. A Photovoltaic Solar Water Heating System, J. Sol. Energy Eng, 119, 126–133, doi:10.1115/1.2887891

Frank, E., Feuerstein, M., Minder, S., and & AG, N. S.: Parabolrinnenkollektoren für Prozesswärme in Schweizer Molkereien, 2013.

Haller, M., Peres, B., Bales, C., Paavilainen, J., Dalibard, A., Fischer, S., Bertram, E., 2013. TRNSYS Type 832 v5.01 "Dynamic Collector Model by Bengt Perers" Updated Input-Output Reference

Heimrath, R. and Haller, M., 2007. The Reference Heating System, the Template Solar System. A technical report of Subtask A. A Report of IEA-SHC Task 32. Institute of Thermal Engineering, Division Solar Energy and Thermal Building Simulation, Graz University of Technology, Graz, Austria

ISO, E. (2013). 9806: 2013. Solar energy–Solar thermal collectors–Test methods.

Lauterbach, Christoph, 2014. Potential, system analysis and preliminary design of low-temperature solar process heat systems. PhD Dissertation, University of Kassel

Le Berre, R., Dupeyrat, P., Plotton, A., Doucet, J.-F., and Lindsay, A., 2014. PV Domestic Hot Water System, EuroSun Proceedings, Aix-les-Bains, France

Shah, V. and Booream-Phelps, J.,2015. Crossing the Chasm: Solar Grid Parity in a Low Oil Price Era, Deutsche Bank

Standard, B. S., & EN, B. (2006). EN 12975-2: 2006, Thermal solar systems and components. Solar collectors. Test methods

Verein Deutscher Ingenieure (VDI), 2014. 6002 - Solar heating of potable water, Basic principles